

## Graphene-based Magnetic Janus Micromotors for Dynamic Removal of Persistent Organic Pollutants

*Jahir Orozco, Luiza A. Mercante, Roberto Pol, Arben Merkoçi\**

Dr. J. Orozco, Dr. L. A. Mercante, R. Pol, Prof. A. Merkoçi  
Nanobioelectronics and Biosensor Group, Catalan Institute of Nanoscience and Nanotechnology (ICN2), CSIC and The Barcelona Institute of Science and Technology, Campus UAB, Bellaterra, 08193, Barcelona, Spain  
E-mail: arben.merkoci@icn.cat

Dr. L. A. Mercante  
National Laboratory for Nanotechnology in Agribusiness (LNNA), Embrapa Instrumentation, 13560-970, São Carlos, SP, Brazil

Prof. A. Merkoçi  
ICREA – Catalan Institution for Research and Advanced Studies, Barcelona, 08010, Spain

**Keywords:** Janus micromotors, graphene, persistent organic pollutants, PBDEs, triclosan

Persistent organic pollutants (POPs) are ubiquitous in the environment as a result of modern industrial processes. We present an effective POPs decontamination strategy based on its dynamic adsorption at the surface of reduced graphene oxide (rGO)-coated silica (SiO<sub>2</sub>)-Pt Janus magnetic micromotors for their proper final disposition. While the motors rapidly move in a contaminated solution, the adsorption of POPs is efficiently taking place in a very short time. Characterization of the micromotors both from the materials and from the motion point of view was performed. Polybrominated diphenyl ethers (PBDEs) and 5-chloro-2-(2,4-dichlorophenoxy) phenol (triclosan) were chosen as model POPs and the efficient removal of the contaminants achieved in only 10 min. rGO-coated micromotors demonstrated to have superior adsorbent properties respect to the concomitant GO-coated micromotors, static rGO-coated particles and dynamic silica micromotors counterparts. The extent of decontamination was studied upon number of micromotors, whose magnetic properties were used for their collection from environmental samples. The adsorption properties were kept for 4 cycles of micromotors reuse. The new rGO-coated SiO<sub>2</sub> functional

material-based micromotors showed outstanding capabilities for removal of POPs and their further disposition, opening up new possibilities for the efficient environmental remediation of these hazardous compounds.

## 1. Introduction

Persistent organic pollutants (POPs) are one of the most troublesome hazardous compounds wide-spread in the environment as residual products of modern industrial processes, remaining in the environment for long time.<sup>[1]</sup> For instance, polybrominated diphenyl ethers (PBDEs) are commonly incorporated as flame-retardants into many products (plastics, electronics, textiles, furniture and carpets).<sup>[2]</sup> 5-chloro-2-(2,4-dichlorophenoxy) phenol (triclosan) is often added in personal care products (deodorants, toothpastes, soaps), clothing and trash bags as antibacterial of broad spectrum.<sup>[3]</sup> Concerns about the environmental impact of these POPs are derived from their widespread use and subsequent residual persistence that is inherent to their physicochemical properties, including high stability, resistance to degradation and lipid solubility.<sup>[4]</sup> In this context, attempts to develop novel methods not only for accurate detection but also for efficient remediation of POPs are worthy of being explored.

Micro/Nanomotors have shown to offer unprecedented potential for a broad range of (bio)chemical science and industrial applications.<sup>[5,6]</sup> For example, it has been demonstrated how the motion of self-propelled micromotors promoted the enhancement of analyte reaction-diffusion and solution accelerated mixing with interest not only in biosensing,<sup>[7]</sup> but also in stirring-free water decontamination strategies.<sup>[8]</sup> The outstanding competences of micromotors for environmental remediation have been recently highlighted in some reviews.<sup>[9,10]</sup> Not only tubular catalytically propelled motors<sup>[8,11,12]</sup> but also Janus particle-based micromotors have been used for decontamination of organic pollutants.<sup>[13-16]</sup> These Janus micromotors comprise a surface of two different faces, each one exhibiting different physicochemical properties. Commonly, one of the faces is responsible of the propulsion, being the other one functionalized (or not) able to perform a

particular remedial task. Novel Janus micromotors based on silver exchanged-zeolite/Pt and Mg/TiO<sub>2</sub> have been proven for the effective and rapid elimination of chemical and biological threats.<sup>[14,15]</sup> Charcol/Pt Janus micromotors were also reported for the dynamic adsorption of a variety of pollutants ranging from heavy metals and nitroaromatic explosives to organophosphorous nerve agents and azo-dye compounds.<sup>[13]</sup> Graphene-wrapped Janus micromotors were used to elucidate the mechanism that governs their motion<sup>[17]</sup> and to study their motion upon the influence of an applied electric field, a chemical potential gradient and an external magnetic field.<sup>[18]</sup> Yet, this is the first exploration of graphene-based micromotors for a dynamic environmental remediation process.

Graphene-based materials have properties that are being harnessed for pollutant enrichment. For example their chemical stability, reduced cytotoxicity, large surface area (low density), high hydrophobic surface, large delocalized  $\pi$  electrons and large scale production possibilities are being exploited in the adsorption of contaminants, including dyes, organic pollutants and even metals.<sup>[19–24]</sup> The use of graphene nanosheets for the adsorption of POPs in water has been recently explored.<sup>[23,25]</sup> Adsorption capacity strongly depends on the graphene available sites to link the organic pollutants, mostly through  $\pi$ - $\pi$  stacking interactions, and on the graphene nanosheets homogeneous dispersity in aqueous media. While the variety of oxygen functionalities of graphene oxide (GO) such as hydroxyl, carboxyl, and epoxy groups provide the material with hydrophilicity, at the same time arrange for a weak  $\pi$  electron structure that result in a poor affinity for aromatic organic pollutants. Reduction of graphene oxide (forming rGO) is a procedure that allows for recovering the adsorption capabilities of GO by giving back its hydrophobic character and  $\pi$  delocalized electron structure. Nevertheless, rGO nanosheets trend to aggregate due to large-area  $\pi$ - $\pi$  interactions and strong van der Waals interactions between the graphene layers, thereby reducing the number of potential adsorption sites of graphene.<sup>[26]</sup> Loading rGO nanosheets onto low-cost substrates/carriers is a promising alternative to overcome such undesirable aggregation. Cheap,

innocuous and abundant silica ( $\text{SiO}_2$ ) is an ideal framework material to support rGO nanosheets preventing their aggregation. Accordingly, adsorption capabilities of rGO-coated  $\text{SiO}_2$  composite materials ( $\text{SiO}_2$ @rGO) are worthy of interrogation for the efficient POPs remediation.

Herein, we present a rapid and efficient POPs decontamination strategy based on adsorption of the POPs at the surface of  $\text{SiO}_2$ @rGO-Pt Janus micromotors. The Janus micromotors are made up of a catalytic Pt layer hemisphere placed at a silica-graphene core-shell-like magnetic microparticle. While the Pt face efficiently self-propels the motors in a POPs contaminated solution the adsorption of these hazard compounds is efficiently taken place at their rGO face in a very short time. The as-prepared micromotors were characterized in terms of materials and motion. PBDE and triclosan were chosen as model POPs and 10 ppb of a contaminated solution were decontaminated in 91 and 89 %, respectively in only 10 min. Control experiments demonstrated that the rGO-coated micromotors adsorbed more pollutants in their surface when compared to the concomitant GO-coated micromotors, static GO-coated particles and dynamic silica micromotors counterparts. The extent of decontamination was studied upon number of motors present in the contaminated solution, and adsorption isotherms and kinetic parameters of the decontamination process were also found. The fact of having the graphene adsorption sites fully expressed at the surface of a cheap, innocuous and magnetic silica-based substrate offers the possibility not only of an efficient POPs removal process but also of its easy collection from an environmental matrix by magnetic means. Successfully POPs removal was achieved for 4 consecutive cycles of micromotors reuse. The new  $\text{SiO}_2$ @rGO functional material-based micromotor demonstrated outstanding capabilities for POPs removal, which open up new possibilities for dynamic environmental remediation.

## 2. Results and discussion

We present a micromotor for the dynamic removal of POPs from contaminated samples. The Janus micromotor consists of two-dimensional rGO nanometric layers/flakes stabilized at a

three-dimensional SiO<sub>2</sub> micrometric 'green structure' and an hemispheric Pt thin layer used for POPs adsorption and micromotor propulsion, respectively. The microparticle substrate comprises some  $\gamma$ -Fe<sub>2</sub>O<sub>3</sub> nanoparticles-containing a NH<sub>2</sub>-SiO<sub>2</sub> core, with a spherical shape of  $5.6 \pm 0.8 \mu\text{m}$  average size, prepared as reported previously.<sup>[27]</sup> The micromotors fabrication process is presented in **Figure 1A** and detailed in both the S.I. Experimental Section and **Figure S1**. Figure 1A shows a sketch of the steps involved in the fabrication process, which comprises the coating of the silica core with a GO layer (1), reduction of the resulting GO-coated microparticle (2) and final recovering of the as-prepared rGO-coated silica particle with a Pt catalytic layer (3). Loading of GO onto the microparticles is achieved through electrostatic interactions coming from the opposite charge of NH<sub>2</sub>-SiO<sub>2</sub> substrate and GO nanosheets at neutral pH, as confirmed by Zeta potential analysis (**Figure S2**). Posterior reduction of the GO-coated microparticles is chemically achieved with the environmental friendly ascorbic acid-based method, following the procedure reported in the literature.<sup>[28,29]</sup> Such reduction imposes again a hydrophobic character to the coating that allows for recovering the  $\pi$  electron structure, while keeping their adsorption places completely exposed at the whole surface.<sup>[23]</sup> Such reduction will improve the adsorption capabilities of the coating, as will be demonstrated later in the removal experiments. rGO-coated SiO<sub>2</sub> microparticles were turned into microengines by covering the upper part of their surface (half part of the particle exposed to the coating process) with a 60 nm hemispheric Pt catalytic layer. Current intensity (deposition rate) and thickness of the layer were tuned to get optimal motion of the micromotors (see details in the S.I. Experimental Section). The superior adsorption capabilities of rGO are promoted by the micromotor motion in a contaminated solution, which results in an enhanced POPs removal capacity. Furthermore, the  $\gamma$ -Fe<sub>2</sub>O<sub>3</sub> nanoparticles render the motors magnetic properties that offer the possibility of their complete collection from a sample after the POPs adsorption process. Zeta-potential of the particles were measured during the different steps of the fabrication process to trace the surface charge changes involved (Figure S2). An initial NH<sub>2</sub>-SiO<sub>2</sub> surface charge of  $+16.9 \pm 0.3$

mV (due to the coating amino groups) was reversed to  $-41.4 \pm 1.2$  mV after GO self-assembly, indicating the negative charges from the GO sheets are predominating on the resulting particle surface. However, after the microparticle reduction process the zeta potential changed to  $-28.4 \pm 0.4$  mV. Such negative charge indicates that chemical reduction cannot fully eliminate the oxygen moieties and SiO<sub>2</sub>@rGO microparticles still contain some residual oxygen functional groups. After the Pt-half covering the negative charge slightly shifted to  $-22.8 \pm 1.6$  mV, demonstrating that such Pt covering has only a little effect on the resultant micromotor electrical character. Topology of the particles was studied in the different steps of the fabrication process by scanning electron microscopy (SEM). **Figure 1Ba** shows the backscattered electron SEM image of a NH<sub>2</sub>-SiO<sub>2</sub> microparticle rough surface, with no apparent difference respect its homologous rGO monolayer-coated SiO<sub>2</sub> one (**Figure 1Bb**). However, in the high-resolution SEM images (Figure 1Ba and b, bottom part) a clear difference in topography is observed. While the NH<sub>2</sub>-SiO<sub>2</sub> (a) has a homogeneously distributed roughness, the rGO-coated SiO<sub>2</sub> microparticle surface (b) shows corrugated and scrolled nanosheets that resemble with some crumples. These closed-up images evidence the GO nanosheets where successfully assembled at the silica substrate (through electrostatic interactions as expected). **Figure 1Bc** shows a rGO-coated SiO<sub>2</sub> particle half-covered with Pt. The fact that around half of the surface appears brighter is an indication of the successful Janus micromotor fabrication. Heavier elements (Pt) backscatter electrons more strongly than light elements (C, O), thus contrasting two well-defined areas of the particle with different chemical composition. The zoomed-in image (Figure 1Bc, bottom part) shows the cracked surface of Pt deposited at the top of the rGO-coated SiO<sub>2</sub> microparticle, necessary for the Janus micromotor propulsion. **Figure 1C** depicts a sketch of the decontamination process strategy, achieved by means of Janus micromotors propelled in a POP solution, where quantification of the amount of POPs after and before the removal process allows for estimation of the decontamination extent.

**Figure 2A** shows the energy-dispersive X-ray (EDX) spectroscopy images illustrating the distribution of the Si, O, Fe and Pt elements in the  $\gamma$ -Fe<sub>2</sub>O<sub>3</sub> nanoparticles-containing SiO<sub>2</sub> inner core and the Pt catalytic patch, respectively. To better understand the chemical composition of the particles coating (GO or rGO), Fourier transform infrared spectroscopy (FTIR) studies were further performed (**Figure 2B**). Loading of the NH<sub>2</sub>-SiO<sub>2</sub> particles with GO and their posterior reduction led to a clearly differentiated FTIR spectra that reflects the different chemical composition of the particles surface. For instance, the broad band between 3200–3400 cm<sup>-1</sup> and the peak at 1638 cm<sup>-1</sup>, attributed to -OH and O-H stretching vibrations,<sup>[30]</sup> respectively are prominent in the NH<sub>2</sub>-SiO<sub>2</sub> particles (a), and decreased as GO sheets were assembled at the microparticles (b) and further reduced (c). The peak at 1735 cm<sup>-1</sup> characteristic of C=O in carboxylic acids is absent in the particles spectrum (a) and higher in the GO-coated microparticles (b) respect to the rGO-coated ones (c). In the same fashion, other peaks such as those at 1211 and 1372 cm<sup>-1</sup> characteristics of epoxy C-O and carboxyl O=C-O stretching vibrations, respectively do not appear in (a), while are higher in (b) respect to (c).<sup>[31]</sup> Overall, the decrease in number and intensity of the peaks in rGO-coated particles (c) respect to the corresponding GO-coated ones counterparts (b) indicates that the reduction process is eliminating many oxygen-containing groups, despite they are not completely eradicated from the surface. The peaks at 1080 and 450 cm<sup>-1</sup>, related with Si-O-Si and Fe-O stretching vibrations, respectively are consistent in the three spectra due to the common  $\gamma$ -Fe<sub>2</sub>O<sub>3</sub>-containing silica structure of the three different materials compared here.

Micromotors were then characterized in terms of their motion. In the absence of H<sub>2</sub>O<sub>2</sub> fuel, needed for micromotors propulsion, the SiO<sub>2</sub>@rGO-Pt micromotors (**Video S1**, right side) hardly display random walks due to Brownian motion. However, in the presence of H<sub>2</sub>O<sub>2</sub> fuel (**Video S1**, left side), the Pt catalytic surface of SiO<sub>2</sub>@rGO-Pt promotes effective oxygen microbubbles evolution that generates a net momentum (directional thrust) that overcomes the Brownian motion, thus propelling the motor in one direction. **Figure 3A** (time-lapse image, upper part) shows the

dramatic increase on the speed of a self-propelled SiO<sub>2</sub>@rGO-Pt magnetic Janus micromotor in the presence of fuel, respect to the micromotor hardly moving with only Brownian motion in absence of it (Figure 3A, bottom part). Micromotors speed shown to be very dependent on the H<sub>2</sub>O<sub>2</sub> fuel concentrations (see details in S.I. Experimental Section). While the micromotor can move at an ultrafast speed of  $725 \pm 42 \mu\text{m s}^{-1}$  at 10 % H<sub>2</sub>O<sub>2</sub> fuel concentration, they only move at  $140 \pm 15 \mu\text{m s}^{-1}$  at 1.5 % fuel concentration (**Figure 3B**). **Video S2** shows the dramatic increase on micromotors speed upon increasing concentration of H<sub>2</sub>O<sub>2</sub> fuel (up to 10 %). The driving force of the micromotors was calculated with the Stokes' drag expression for spherical colloids at low Reynolds number, *i.e.*  $F = 6\pi\mu r v$ ,<sup>[32]</sup> where  $r$  is the radius of the sphere,  $v$  is the speed of the micromotor, and  $\mu$  is the dynamic viscosity of water. The Janus micromotors (at 10 % H<sub>2</sub>O<sub>2</sub> fuel) achieve an ultrafast speeds that corresponds to a large driving force of 33 pN, comparable with some previous Janus micromotor reports.<sup>[33]</sup> This driving force is amply sufficient to carry small chemical cargo such as PBDEs and triclosan, and even heavier cargo such as magnetic microparticles.<sup>[34,35]</sup> Both, speed and direction, are parameters to be controlled when micromotors are envisioned for real applications.<sup>[36,37]</sup> Herein, magnetic properties of the micromotors, essential to collect them from a sample after a POPs removal process, were also checked. Magnetic Janus micromotors were guided to the edge of a microdrop as a result of the application of a magnetic field from a magnet. When the magnet was tucked off, the micromotors randomly migrated a way of the microdrop edge (**Video S3**), thereby demonstrating the magnetic properties of the micromotors, coming from the  $\gamma$ -Fe<sub>2</sub>O<sub>3</sub> nanoparticles of the micromotors inner core. Efficiency of the Janus micromotors fabrication process in terms of motions was studied by estimating the number of motors that stay active in the presence of different concentrations of fuel, at 3% sodium cholate (NaCh) concentration (**Figure 3C**). Results show that even most of the micromotors vigorously produce bubbles, only up to 91% of the micromotors can move at 10% of H<sub>2</sub>O<sub>2</sub> fuel concentration, while only around half of the population moves at 3% H<sub>2</sub>O<sub>2</sub> fuel. This observation is an indication of the fact that along with the



micromotor motion, bubbling is playing a key role in the diffusion of the pollutant towards the micromotors and further adsorption at their surface.<sup>[8]</sup> Over bubbles production showed to overflow the removal container and would expect to have an adverse effect on the POPs adsorption process. Based on the aforementioned results, minimal fuel and surfactant concentrations down to 1.5 and 3% were selected as optimal conditions for the decontamination experiments, which resulted to be enough for an efficient removal of POPs, as demonstrated later.

A set of experiments was conducted to demonstrate the enhanced capabilities of the SiO<sub>2</sub>@rGO-Pt Janus micromotors for removal of POPs. Quantification of the amount of POP after and before the micromotor-accelerated removal process is achieved by using the commercial Abraxis PBDEs and triclosan assays. The kits principle relies on a competitive assay where the target (each POP) is competing with an enzyme-labelled homologous target for the binding sites at some POP-antibodies specific paramagnetic particles, following the scheme of an enzyme linked immunosorbent assay (ELISA).<sup>[38]</sup> **Figure 4A** shows the absorbance spectra of PBDEs (left) and triclosan (right) POPs removal experiments when  $1 \times 10^6$  micromotors navigated in a 10 ppb contaminated solution for 10 min. The micromotor decontaminated solutions show spectra (dotted blue lines) which intensities are much higher than those from the contaminated ones (dashed red lines) and very close to those from the initial clean solutions (black continuous lines), respectively, as per the competitive immunoassay-based quantification method. From the spectra, the extent of removal were calculated to be  $91.0 \pm 3.4$  and  $87.0 \pm 2.9$  % for PBDEs (left) and triclosan (right), respectively. These similar extents are consistent with the similar molecular structures of the POPs interrogated. The two aromatic rings, common in both structures, are the ones responsible of the  $\pi$ - $\pi$  staking interactions with the rGO micromotors outermost surface cover. Further increase in the micromotors number can lead to both higher removal extents and/or adsorption of higher POPs concentrations. In this context, the extent of decontamination was studied upon the number of motors (**Figure 4B**, left side). When the amount of motors were increased up to  $1.5 \times 10^6$ , the

extent of removal went up to  $97.0 \pm 2.9$  %. These results demonstrated that the quantity of micromotors to be placed in a contaminated solution can be tailored depending on the grade of contamination of the sample and its volume. The extent of PBDEs removal of SiO<sub>2</sub>@rGO-Pt Janus micromotors were compared to those obtained with silica-coated graphene oxide micromotors (SiO<sub>2</sub>@GO-Pt), silica-coated reduced graphene oxide static microparticles (SiO<sub>2</sub>@rGO) and silica micromotors (SiO<sub>2</sub>-Pt), respectively, when using the same micromotors number in the POP contaminated solution (Figure 4B, right). The enhanced adsorption achieved with the SiO<sub>2</sub>@rGO-Pt Janus micromotors ( $91.0 \pm 2.9$  %) not only significantly decreased with the increase of oxygen groups in the outermost graphene nanosheets, *i.e.* the SiO<sub>2</sub>@GO-Pt Janus micromotors ( $65.0 \pm 4.1$  %), but also dramatically decreased when the reduced graphene nanosheets-coated microparticles (SiO<sub>2</sub>@rGO) were quiescent in the contaminated solution ( $23.0 \pm 2.8$  %). These results suggest that the superior adsorption capabilities and corresponding POP removal high extent of the Janus micromotors are due to the synergistic effect of the highly hydrophobic character and the strong potential  $\pi$ - $\pi$  stacking interactions of the exposed reduced graphene nanosheets,<sup>[23]</sup> combined with the enriched adsorption of the pollutants that is promoted by the enhanced mass transport from the micromotors motion.<sup>[13]</sup> In contrast, the SiO<sub>2</sub>-Pt micromotors showed poor adsorption ability towards the POPs ( $12.0 \pm 3.7$  %), which is in agreement with their hydrophilic surface.<sup>[30]</sup>

To gain further insight into the adsorption mechanism, adsorption capacity of the micromotors (adsorbent) was then studied upon time. The removal extent of PBDEs (adsorbate) is increasing upon time at the time range studied (1-10 min) and decreasing as concentration of PBDEs went from 5 (a), to 10 (b) and 20 (c) ppb, respectively, for the same amount of SiO<sub>2</sub>@rGO-Pt Janus micromotors (**Figure 5A**). The mass of PBDEs adsorbed at the micromotors surface was estimated from the removal extend graph and Langmuir and Freundlich adsorption isotherms plotted at the system equilibrium state,  $t = 10$  min (**Figure S3**). The Langmuir and Freundlich

models are giving by the **Equation 1** and **2**, respectively. Where  $q_e$  is the amount of adsorbate per unit of adsorbent ( $\text{mg g}^{-1}$ ),  $C_e$  is the adsorbate equilibrium concentration ( $\text{mg l}^{-1}$ ),  $Q$  and  $b$  (Langmuir constants) and  $K_f$  and  $n$  (Freundlich constants) are related to adsorption capacity ( $Q$  and  $K_f$ ) and rate of adsorption ( $b$  and  $n$ ), respectively.

$$\frac{1}{q_e} = \frac{1}{Q} + \frac{1}{QbC_e} \quad (1)$$

$$\ln q_e = \frac{1}{n} \ln C_e + \ln K_f \quad (2)$$

When plotting  $1/q_e$  vs  $1/C_e$  (Langmuir) and  $\ln q_e$  vs  $\ln C_e$  (Freundlich) we found that the data fit slightly better the Freundlich isotherm model with a correlation coefficient  $R^2$  of 0.9996, respect to 0.9982 from the Langmuir model (see Figure S3). These results suggest that unlike uniform adsorption, the adsorbate adsorption takes place on a heterogeneous surface at sites with different energy of adsorption. This is in agreement with the different graphene surface-energy adsorption sites, as compared to flatter surfaces.<sup>[23]</sup> From the fitted date,  $K_f$  and  $n$  were calculated to be  $3.257 (\text{mg g}^{-1})(1 \text{ mg}^{-1})^n$  and 1.14, respectively. Such  $K_f$  value is much higher compared to that estimated from some  $\text{NH}_2\text{-SiO}_2$  nanoparticles (0.0048), slightly higher respect to that from the particles decorated with some rGO nanosheets (1.7371) and much lower compared to only pristine graphene (149.26), as expected; all of them adsorbing phenanthrene POP at their corresponding static particle surface.<sup>[30]</sup> The  $n$  value, greater than unity, indicates that the PBDEs is favourably adsorbed at the  $\text{SiO}_2\text{@rGO-Pt}$  micromotors surface. The rate constant of adsorption was determined from the pseudo-first-order equation given by Langergren and Svenska (**Equation 3**) and from a pseudo-second-order equation based on equilibrium adsorption (**Equation 4**), respectively, where  $q_e$  is the sorption capacity at equilibrium and  $q_t$  is the loading of POP at time  $t$ . The parameters  $k_1$  and  $k_2$  ( $\text{g} (\text{mg min})^{-1}$ ) represents the pseudo-first- and pseudo-second-order rate constants for the kinetic models, respectively. The slope and intercept of the linear plots from Equation 3 and 4 yield the

values of  $q_e$  and  $k_2$ . The linear plots of  $\ln q_e$  vs  $t$  and  $t/q_t$  versus  $t$  (**Figure 5B**) for 5 (a), 10 (b) and 20 (c) ppb, respectively show that data fit much better the pseudo-second-order kinetic model, indicating that chemisorption of PBDEs at the SiO<sub>2</sub>@rGO-Pt micromotors surface is the rate determining step (see additional information in **Table S1**). These results are in agreement with the kinetic model estimated for some POP at a GO adsorbent surface.<sup>[39]</sup>

$$\ln q_e = \ln (q_e - q_t) + k_1 t \quad (3)$$

$$\frac{t}{q_t} = \frac{1}{K_2 q_e^2} + \left(\frac{1}{q_e}\right) t \quad (4)$$

To test the effect of an environmental matrix on the removal process, towards demonstrate the practical utility of the SiO<sub>2</sub>@rGO-Pt micromotors, we interrogated the removal extent of POPs in a seawater samples. **Figure 6A** (left side) shows the spectra of the PBDEs removal (doted blue line), which intensity is higher than that from the spiked POP-seawater sample (dash red line), consistent with the competitive immunoassay used herein as quantification method, and nearer to that from the initial unpolluted solution (black continuous line), respectively. From the spectra, the extent of removal was calculated to be  $76 \pm 2.8$  %. The slightly lower extent, respect to that estimated from POP-spiked deionized water might be related with some matrix effects.  $\pi$ - $\pi$  interactions between the rGO micromotors coating and some organic compounds that may eventually be present in the environmental sample might be accounting for such lower removal extent. Indeed, the micromotors speed in a contaminated solution containing 33% of seawater slows down to  $100 \pm 33 \mu\text{m s}^{-1}$  (**Video S4**). Such slower motion, in respect to the motion in a water sample ( $725 \pm 42 \mu\text{m s}^{-1}$ ) might be also accounting for the decrease in the removal extent. In a similar fashion, the extent of removal was also studied for a seawater sample where both PBDEs

and triclosan are present. For this purpose a 5 ppb PBDEs and 5 ppb triclosan mixture were spiked in the seawater sample (Figure 6A, right side), and the extent of decontamination were calculated after the SiO<sub>2</sub>@rGO-Pt micromotors-based accelerated removal. Quantification of PBDEs and triclosan in the mixture was separately achieved by using the corresponding kits (see S.I. Experimental Section). As both kits are based on the same immunodetection principle and they have shown to interfere with one another, we first estimated the effect of triclosan over PBDEs quantification and later the one of PBDEs over the triclosan quantification (see details in S.I. Experimental Section). We found that when quantifying PBDEs in the presence of triclosan the concentration was overestimated in a 1.20 factor and when triclosan was quantified in the presence of PBDEs the concentration was overestimated in a 1.15 factor, in agreement with the literature.<sup>[38,40]</sup> The corresponding spectra were then normalized respect the empirically found factors when coexisting both POPs in the same seawater sample as shown in Figure 6A, right side. The dotted blue and cyan lines are the normalized spectra for the removal of PBDEs coexisting with triclosan and vice versa, respectively respect to the spectra from the initial clean solution (continuous black line). The removal extents were estimated to be  $74 \pm 2.1$  and  $71 \pm 3.2$  %, for PBDEs and triclosan, respectively. The removal extent of PBDEs when coexists with triclosan is quite similar to that obtained from PBDEs alone in the seawater sample and significantly lower when compared to that from deionized water. Yet, the removal extent can be potentially improved in real samples by slightly increasing the number of motors (Figure 4B, left) or the removal time (Figure 5A) depending on the concentration of POPs, as demonstrated for deionized water. These results indicated that adsorption capabilities of the micromotors towards the POPs are very promising for removal of these pollutants from real environmental samples and other contaminated samples. Therefore, such improved capabilities combined to the magnetic properties of the Janus micromotors can be exploited in the efficient adsorption of pollutants for their final disposal.

The ideal adsorbent material not only must have a high adsorption capability, but also should show desorption properties to be reused. Having in mind a water remediation practical application based on the micromotors adsorption capacity, we evaluated the recycling ability of the SiO<sub>2</sub>@rGO-Pt micromotors while removing POPs. Pollutants adsorbed at porous graphene-based materials have been desorbed by heat, acidic and electric treatment, among other desorption methods.<sup>[39]</sup> However, they may produce some further harming of the environment. One of the advantages of the moving adsorption platform proposed herein is its high stability from the structural and chemical point of view, which offers the possibility of regeneration cycles after each micromotors use by simply desorbing the adsorbed pollutants from them. Herein, reusability was studied based on the  $\pm 3\sigma$  criterion. Herein, a control chart (**Figure 6B**) was plotted taking the mean value of the micromotor-based removal extent from successive measurements the first day of the study, considered as central value. The upper and lower control limits were set at three times the standard deviation of this value. The micromotor-based adsorbent platform was reused until the removal extent was lower than 3-folds the standard deviation of the removal measurements from the first cycle. Based on this criterion, the micromotors were reused for 4 cycles (Figure 6B) with a desorption step in between cycles performed in isoctane solvent as detailed in the S.I. Experimental Section. The micromotors magnetic properties were crucial not only for their magnetic separation in the reusability experiments, but also offers an alternative for the final disposition of the adsorbed pollutants after their removal from real environmental samples.

### 3. Conclusion

We have presented a SiO<sub>2</sub>@rGO-Pt Janus micromotors-based strategy for the enhanced removal of PBDEs and triclosan POPs from environmental samples. These hazards pollutants were rapidly adsorbed at the outermost rGO coating from the micromotors while they were autonomously propelled in the contaminated solution. The reduced graphene coating demonstrated

to have superior adsorption capabilities than its homologous graphene oxide form. In the same fashion, the dynamic adsorption of the POPs by the micromotors led to an enhanced removal extent when compared to the corresponding static counterparts. The synergistic effect of the superior adsorbent properties of the micromotor coating, along with the enhanced adsorbate/adsorbent interaction -promoted by the micromotor motion- led to an improved removal extent of around 90% of POPs in only 10 min. The approach presented here can be explored in the decontamination of some other aromatic-containing pollutants whether conditions tailored by varying the number of micromotors and interaction time, based on the pollutants concentration. The adsorption mechanism has shown to adjust better with the Freundlich model, following a pseudo-second-order kinetics, thereby indicating that chemisorption of POPs at the heterogeneous graphene-wrapped micromotors surface is the rate determining step. The magnetic properties of the micromotors were exploited to collect them from the environmental sample after the removal process. Successfully removal was achieved for 4 consecutive cycles. Overall, the new SiO<sub>2</sub>@rGO functional material-based micromotor demonstrated outstanding capabilities for POPs removal, which open up new ways of dynamic environmental remediation of these troublesome hazardous compounds.

### **Supporting Information**

Supporting Information is available from the Wiley Online Library or from the author.

### **Acknowledgements**

This work was supported by the European Commission Program, FP7-OCEAN, SMS Project (613844). ICN2 acknowledges support from the Severo Ochoa Program (MINECO, Grant SEV-2013-0295). Nanobiosensors and Bioelectronics Group acknowledges the support from Generalitat de Catalunya (Grant 2014 SGR 260). L.A.M acknowledges financial support from FAPESP-BEPE (2014/26088-4) project. D. Horák and B.A. Zasońska, from Institute of Macromolecular Chemistry

(Czech Republic), are acknowledged for providing us with the SiO<sub>2</sub> microparticles. Authors also thank E. Morales for his wise advices.

Received: ((will be filled in by the editorial staff))

Revised: ((will be filled in by the editorial staff))

Published online: ((will be filled in by the editorial staff))

- [1] K. Jones, P. De Voogt, *Environ. Pollut.* **1999**, *100*, 209.
- [2] A. Covaci, S. Harrad, M. A.-E. Abdallah, N. Ali, R. J. Law, D. Herzke, C. A. de Wit, *Environ. Int.* **2011**, *37*, 532.
- [3] G. S. Dhillon, S. Kaur, R. Pulicharla, S. K. Brar, M. Cledón, M. Verma, R. Y. Surampalli, *Int. J. Environ. Res. Public Health* **2015**, *12*, 5657.
- [4] M. S. El-Shahawi, A. Hamza, A. S. Bashammakh, W. T. Al-Saggaf, *Talanta* **2010**, *80*, 1587.
- [5] M. Guix, C. Mayorga-Martinez, A. Merkoçi, *Chem. Rev.* **2014**, *114*, 6285.
- [6] X. Lin, Z. Wu, Y. Wu, M. Xuan, Q. He, *Adv. Mater.* **2015**, *1*.
- [7] E. Morales-Narváez, M. Guix, M. Medina-Sánchez, C. C. Mayorga-Martinez, A. Merkoçi, *Small* **2014**, *10*, 2542.
- [8] J. Orozco, G. Cheng, D. Vilela, S. Sattayasamitsathit, R. Vazquez-Duhalt, G. Valdés-Ramírez, O. S. Pak, A. Escarpa, C. Kan, J. Wang, *Angew. Chemie Int. Ed.* **2013**, *52*, 13276.
- [9] L. Soler, S. Sánchez, *Nanoscale* **2014**, *6*, 7175.
- [10] W. Gao, J. Wang, *ACS Nano* **2014**, *8*, 3170.
- [11] L. Soler, V. Magdanz, V. Fomin, S. Sánchez, O. Schmidt, *ACS Nano* **2013**, *7*, 9611.
- [12] J. Orozco, D. Vilela, G. Valdés-Ramírez, Y. Fedorak, A. Escarpa, R. Vazquez-Duhalt, J. Wang, *Chem. - A Eur. J.* **2014**, *20*, 2866.
- [13] B. Jurado-Sánchez, S. Sattayasamitsathit, W. Gao, L. Santos, Y. Fedorak, V. V. Singh, J. Orozco, M. Galarnyk, J. Wang, *Small* **2015**, *11*, 499.
- [14] V. V. Singh, B. Jurado-Sánchez, S. Sattayasamitsathit, J. Orozco, J. Li, M. Galarnyk, Y. Fedorak, J. Wang, *Adv. Funct. Mater.* **2015**, *25*, 2147.



- [15] J. Li, V. V Singh, S. Sattayasamitsathit, J. Orozco, K. Kaufmann, R. Dong, W. Gao, B. Jurado-Sánchez, Y. Fedorak, J. Wang, *ACS Nano* **2014**, *8*, 11118.
- [16] W. Gao, X. Feng, A. Pei, Y. Gu, J. Li, J. Wang, *Nanoscale* **2013**, *5*, 4696.
- [17] X. Ma, J. Katuri, Y. Zeng, Y. Zhao, S. Sánchez, *Small* **2015**, *11*, 5023.
- [18] S. Kumar, A. K. Singh, A. K. Dasmahapatra, T. K. Mandal, D. Bandyopadhyay, *Carbon N. Y.* **2015**, *89*, 31.
- [19] S. M. Maliyekkal, T. S. Sreeprasad, D. Krishnan, S. Kouser, A. K. Mishra, U. V Waghmare, T. Pradeep, *Small* **2013**, *9*, 273.
- [20] E. Morales-Narváez, A.-R. Hassan, A. Merkoçi, *Angew. Chemie Int. Ed.* **2013**, *52*, 13779.
- [21] N. Ding, X. Chen, C. Wu, *Environ. Sci. Nano* **2014**, *55*.
- [22] E. Morales-Narváez, T. Naghdi, E. Zor, A. Merkoçi, *Anal. Chem.* **2015**, *87*, 8573.
- [23] K. Yang, B. Chen, L. Zhu, *Sci. Rep.* **2015**, *5*, 11641.
- [24] G. Zhao, L. Jiang, Y. He, J. Li, H. Dong, X. Wang, W. Hu, *Adv. Mater.* **2011**, *23*, 3959.
- [25] Y. Shen, Q. Fang, B. Chen, *Environ. Sci. Technol.* **2015**, *49*, 67.
- [26] F. Perreault, A. de Faria, M. Elimelech, *Chem. Soc. Rev.* **2015**, *44*, 5861.
- [27] P. Šálek, L. Korecká, D. Horák, E. Petrovský, J. Kovářová, R. Metelka, M. Čadková, Z. Bílková, *J. Mater. Chem.* **2011**, *21*, 14783.
- [28] J. Zhang, H. Yang, G. Shen, P. Cheng, J. Zhang, S. Guo, *Chem. Commun.* **2010**, *46*, 1112.
- [29] S. Eigler, S. Grimm, M. Enzelberger-Heim, P. Müller, A. Hirsch, *Chem. Commun.* **2013**, *49*, 7391.
- [30] K. Yang, J. Wang, B. Chen, *J. Mater. Chem. A* **2014**, *2*, 18219.
- [31] X. Chen, B. Chen, *Environ. Sci. Technol.* **2015**, *49*, 6181.
- [32] E. Lauga, T. R. Powers, *Reports Prog. Phys.* **2009**, *72*, 096601.
- [33] Y. Wu, Z. Wu, X. Lin, Q. He, J. Li, *ACS Nano* **2012**, *6*, 10910.
- [34] L. Baraban, M. Tasinkevych, M. Popescu, S. Sanchez, S. Dietrich, O. Schmidt, *Soft Matter* **2012**, *8*, 48.

- [35] L. Baraban, D. Makarov, I. Mönch, D. Grimm, S. Sanchez, O. G. Schmidt, *ACS Nano* **2012**, *6*, 3383.
- [36] L. Baraban, D. Makarov, O. G. Schmidt, G. Cuniberti, P. Leiderer, A. Erbe, *Nanoscale* **2013**, *5*, 1332.
- [37] J. Palacci, S. Sacanna, A. Vatchinsky, P. M. Chaikin, D. J. Pine, *J. Am. Chem. Soc.* **2013**, *135*, 15978.
- [38] W. Shelver, L. Kamp, J. Church, F. Rubio, *J. Agric. Food Chem.* **2007**, *55*, 3758.
- [39] H. Sun, L. Cao, L. Lu, *Nano Res.* **2011**, *4*, 550.
- [40] L. Kantiani, M. Farré, D. Asperger, F. Rubio, S. González, M. J. López de Alda, M. Petrović, W. L. Shelver, D. Barceló, *J. Hydrol.* **2008**, *361*, 1.

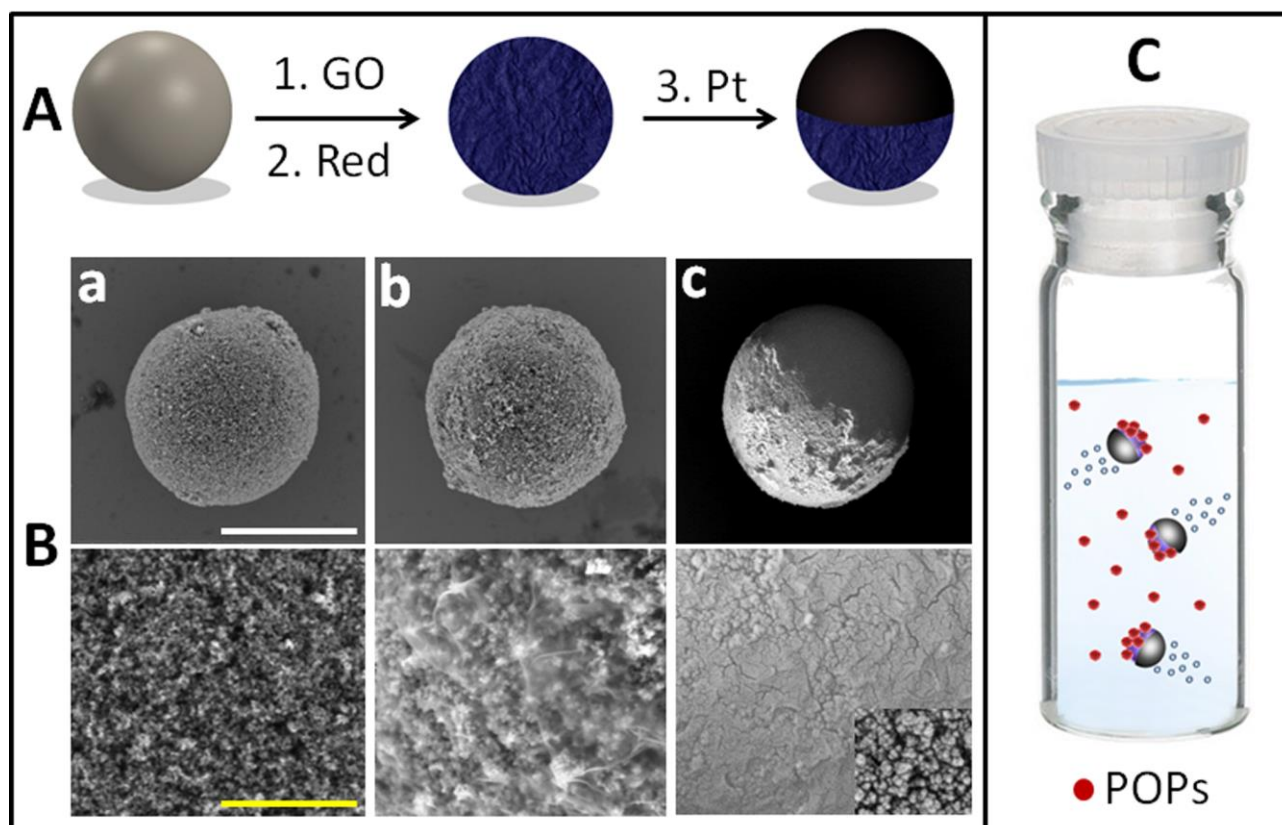


**Figure 1.** Micromotors fabrication process and POPs removal concept. A) Sketch of the steps involved in the fabrication process: 1) coating of a silica particle with graphene oxide (GO), 2) reduction of the GO-coated micromotor, 3) recovering of half of the resulting rGO-coated silica particle with a Pt catalytic layer. B) Backscattered scanning electron microscopy (SEM) images of: a) a silica particle, b) a rGO monolayer-coated silica particle and c) a half covered Pt rGO-coated silica particle. Scale bars are 4  $\mu\text{m}$  (upper line), 500 nm (bottom line). C) Sketch of the decontamination process: some Janus micromotors propelled in a POP solution.

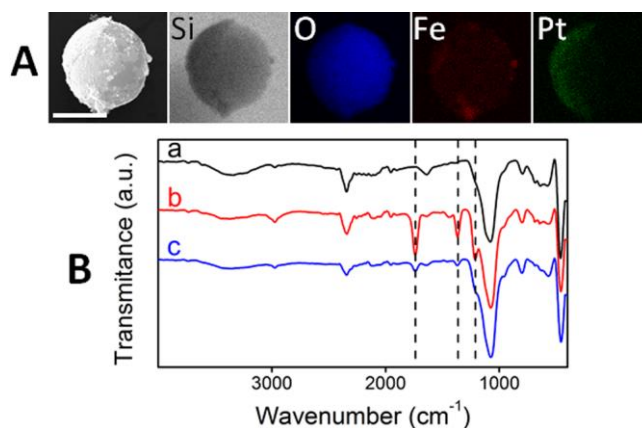


**Figure 2.** Characterization of the micromotors chemical composition. A) Energy-dispersive X-ray (EDX) spectroscopy images illustrating the distribution of the Si, O, Fe and Pt elements in the  $\gamma$ - $\text{Fe}_2\text{O}_3$  nanoparticles-containing  $\text{SiO}_2$  inner core and Pt catalytic patch, respectively. B) Fourier transform infrared (FTIR) absorption spectrum giving information about the chemical composition of GO (b) and rGO (c) coated  $\text{SiO}_2$  microparticles, respect to the concomitant bare  $\text{SiO}_2$  counterparts (a). Scale bar is 4  $\mu\text{m}$ .

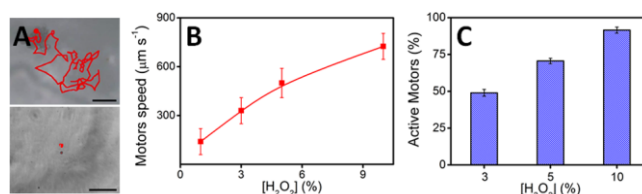


**Figure 3.** Characterization of the micromotors motion. Time-lapse images taken from S.I video 1, of a Janus micromotor moving for 7s in the presence of fuel (A, upper part) respect to a Janus micromotor with no fuel, displaying Brownian motion for the same time (A, bottom part). B) Micromotors speed dependence on the  $\text{H}_2\text{O}_2$  fuel concentration. C) Efficiency of the Janus micromotors fabrication process, estimated as the number of motors that stay active in the presence of different concentrations of fuel. Error bars indicate the standard deviation of 20 measurements. Scale bar is 50  $\mu\text{m}$ .

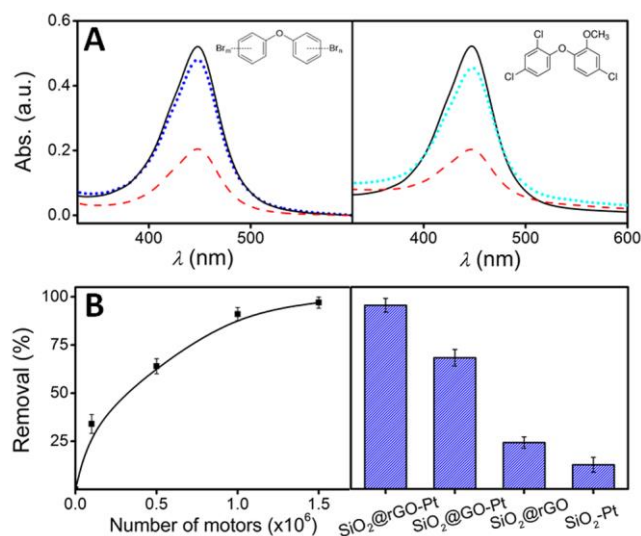


**Figure 4.** Micromotors-based removal of POPs. A) Absorbance spectra of the PBDEs (left) and triclosan (right) POPs: initial clean (continuous black line), contaminated (dashed red line) and decontaminated solutions (dotted blue line), respectively. B) Extent of decontamination upon number of motors (left) and comparison of the extent of decontamination (right) when using silica-coated reduced graphene oxide micromotors (SiO<sub>2</sub>@rGO-Pt), and respect to those obtained with silica-coated graphene oxide micromotors (SiO<sub>2</sub>@GO-Pt), silica-coated reduced graphene oxide static microparticles (SiO<sub>2</sub>@rGO) and silica micromotors (SiO<sub>2</sub>@Pt), respectively. Error bars indicate the standard deviation of three measurements. Conditions: 500 μl of a 10 ppb POP contaminated solution containing, 1.5% H<sub>2</sub>O<sub>2</sub>, 3% NaCh and 1 X 10<sup>6</sup> micromotors.

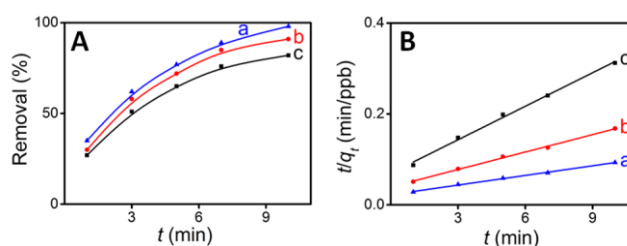


**Figure 5.** A) Adsorption and kinetic studies. Time dependence on the removal extent: 5 (a), 10 (b) and 20 (c) ppb of PBDEs contaminated solutions, by using SiO<sub>2</sub>@rGO-Pt Janus micromotors; and B) corresponding pseudo-second-order kinetic model. Other conditions are as in Figure 4.

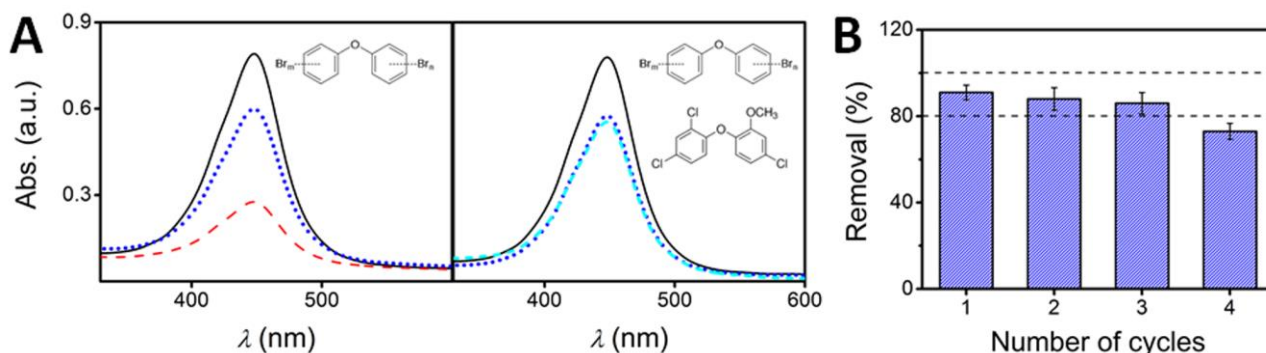
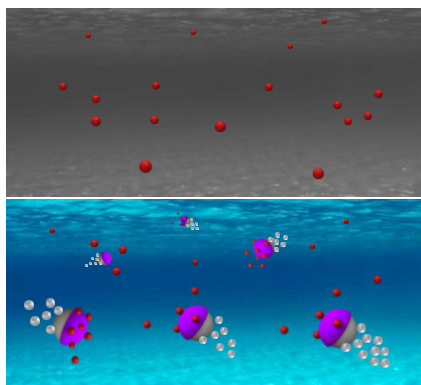


**Figure 6.** Removal of POPs in real environmental samples and micromotors reusability. Removal of POPs from a 10 ppb PBDEs (A, left side); and 5 ppb PBDEs and 5 ppb triclosan mixture in seawater contaminated solutions (A, right side), respectively. Initial concentration of spiked POP in the sample is in a dash red line, uncontaminated samples are in a black continuous line, removal of PBDEs and triclosan are in a dotted blue line and a short dash cyan line, respectively. B) Number of cycles that the same batch of micromotors was used for the removal of 10 ppb PBDEs. Error bars indicate the standard deviation of three measurements. Other conditions are as in Figure 4.

**We present a SiO<sub>2</sub>@rGO-Pt Janus micromotors-based strategy for the enhanced removal of POPs for their proper final disposition.** The synergistic effect of the superior adsorbent properties of the micromotor coating, along with the enhanced adsorbate/adsorbent interaction -promoted by the micromotor motion- led to an improved removal extent of around 90% of POPs in only 10 min.

**Keyword:** Janus micromotors, graphene, persistent organic pollutants, PBDEs, triclosan

Jahir Orozco, Luiza A. Mercante, Roberto Pol, Arben Merkoçi\*



Copyright WILEY-VCH Verlag GmbH & Co. KGaA, 69469 Weinheim, Germany, 2013.

## Supporting Information

### **Graphene-based magnetic Janus micromotors for dynamic removal of persistent organic pollutants**

*Jahir Orozco, Luiza A. Mercante, Roberto Pol, Arben Merkoçi\**

#### **Videos**

**Video S1.** SiO<sub>2</sub>@rGO-Pt micromotors motion vs Brownian motion.

**Video S2.** Effect of H<sub>2</sub>O<sub>2</sub> concentration on the micromotors motion.

**Video S3.** Micromotors magnetic properties. The video is presented in slow motion, at 40% of the real speed.

**Video S4.** Micromotors motion in a seawater sample.

#### **Experimental Section**

*Synthesis of Janus micromotors.* 1 ml of 1.3 mg ml<sup>-1</sup> SiO<sub>2</sub> magnetic microparticles provided by Beata Anna Zasońska and Daniel Horák from Institute of Macromolecular Chemistry (Czech Republic), were washed three times with water and then, 800 µl water were added to the microparticles, followed by 200 µl of a 0.5 wt.% graphene (GO) solution (Angstrom materials). The mixture was stirred at 650 rpm for 2h. The resultant SiO<sub>2</sub>@GO microparticles were washed three times with water before suspend them in 1 ml of 0.3 mgml<sup>-1</sup> ascorbic acid solution for reduction of the GO-wrapped microparticles. The mixture was left stirring at 1200 rpm for 48 h, washed 3 times with deionized water and resuspended in 1 ml of water. To obtain the Pt hemispheric Janus



micromotors, the as-prepared SiO<sub>2</sub>@rGO microparticles were dissolved in 500 µl isopropanol (Sigma-Aldrich) and 150 µl of the solution was placed on top of a glass slide and left them dry at room temperature. Sputtering of Pt was carried out on a Leica EM ACE600. Current intensity (deposition rate) *i.e.* 30, 60 and 90 mA (0.1, 0.23 and 0.46 nm s<sup>-1</sup>), respectively and thickness of the layer (20, 40 and 60 nm) were tuned to get optimal motion of the micromotors. In order to obtain a uniform Janus half-shell coating, the sample slides were set up in parallel to the Pt target. Optimal conditions were settled at 30 mA current, 60 nm Pt layer and a rotation speed of ~18 rpm. Some volume of water were then placed on top of the SiO<sub>2</sub>@rGO-Pt microparticles and the glass slide placed in a sonication bath for short periods of time until most of the particles get released from the surface. The particles are collected in an eppendorf and concentrated up to 10 million of particles ml<sup>-1</sup>.

*Propulsion of Janus micromotor.* The propulsion of micromotors was tested under the microscope. Aqueous solutions of micromotors, sodium cholate (NaCh, Sigma-Aldrich) and H<sub>2</sub>O<sub>2</sub> (Sigma-Aldrich), 2 µl each, were added consecutively on top of a glass slide. Optimal concentration was studied by varying the concentration of H<sub>2</sub>O<sub>2</sub> from 1.5 to 10 %. For testing propulsion of the micromotors in real samples 33% of a seawater sample was used. Videos were captured by an inverted optical microscope (Olympus IX71) coupled with 4X, 20X and 40X objectives, at 20 frames s<sup>-1</sup> and Cellsens software were used for capturing movies and photos. The micromotors speed was tracked using Fiji (ImageJ2) software.

*Removal experiments.* First, a calibration curve for PBDEs and Triclosan was done using a magnetic particle enzyme-linked immunoassay (ELISA) kit (Abraxis).<sup>[2]</sup> 1 ppm Stock solutions of PBDEs (AccuStandard) and 10 ppm stock solution of Triclosan (Sigma-Aldrich) were prepared by diluting the as-received reagents in ethanol and methanol (from Sigma-Aldrich), respectively and stored at 4 °C when not in use. Standard solutions of 0 to 1 ppb of either PBDEs or Triclosan were prepared and the calibration curves obtained by plotting the natural logarithm of the absorbance

relative to the absorbance of the blank vs the natural logarithm of the PBDEs or triclosan concentrations, respectively. Data fit with straight lines with equations:  $y = -0.23 \ln[\text{PBDEs}] - 1.03$  ( $R^2 = 0.996$ ) and  $y = -0.31 \ln[\text{triclosan}] - 1.26$  ( $R^2 = 0.991$ ). Solutions for the remediation experiments were prepared to have final concentrations of 10 ppb of PBDEs (or triclosan),  $10^6$  motors  $\text{ml}^{-1}$ , 3 wt. % of NaCh and 1.5 wt. % of  $\text{H}_2\text{O}_2$ , in a total volume of 500  $\mu\text{l}$ . Remediation experiments were performed by adding the micromotors solution at the bottom of a glass container, already containing the before mentioned solutions (except for the fuel solution). Then, once the fuel is added, the motors were let to propel in the PBDEs (or triclosan) contaminated solution for 10 min. To prevent the inactivation that  $\text{H}_2\text{O}_2$  can produce on the HRP enzyme (from the enzymatic kit) an aliquot of 20  $\mu\text{l}$  of the remediation solution was placed into 80  $\mu\text{l}$  of 325 mM sodium bisulphite (Sigma-Aldrich) solution to eliminate the  $\text{H}_2\text{O}_2$  remaining in the remediation solution. Sodium bisulphite must be in at least double molar ratio respect to the expected  $\text{H}_2\text{O}_2$  remaining concentration.<sup>[3]</sup> Afterwards, the samples were diluted with deionized water to get a concentration of 0.4 ppb and concentration of PBDEs (or triclosan) pollutant was estimated before and after the remediation process, following the steps detailed in the Abraxis kits.

*Removal experiments in real samples.* To study the micromotor-based removal extend either 10 ppb of PBDEs or a mixture of 5 ppb PBDEs and 5 ppb triclosan were spiked in a seawater sample, collected from Icaria shorts, Barcelona (Spain). Quantification of only PBDEs, and of PBDEs and triclosan coexisting in the sample were separately achieved by using the corresponding kits, as explained in the previous section. As both kits are based on the same immunodetection principle and they have shown to interfere with one another, we first estimated the effect of triclosan over PBDEs quantification and later the one of PBDEs over the triclosan quantification. For this purpose we built a calibration curve with increasing concentrations of PBDEs in the presence of a 0.4 ppb fix concentration of triclosan interference and another one with increasing concentrations of triclosan with a 0.4 ppb fix concentration of PBDEs interference. By relating the

curves obtained in the presence of interferences with those obtained without them, we found that PBDEs and triclosan quantification were overestimated in 1.20 and 1.15 factors, respectively when compared to each of the analytes quantified alone. Those factors are in agreement with those reported in the literature.<sup>[2,4]</sup> The corresponding spectra were then normalized respect the empirically found factors when coexisting both POPs in the same seawater sample.

*Reusability experiments.* To check the potential reusability of the SiO<sub>2</sub>@rGO-Pt micromotors, we conducted some successive adsorption–desorption cycles. The micromotors were regenerated by solvent cleaning treatment, using isooctane (Sigma-Aldrich) as solvent. After the first cycle, the micromotors were magnetically separated from the seawater solution and washed twice with 100 µl ethanol before suspend them in 500 µl isooctane for desorption of PBDEs. After 30 min, the particles were separated and washed twice again with ethanol and then reused for the subsequent adsorption and desorption cycle.

*Characterization.* Micromotors scanning electron microscopy (SEM) images and EDS mapping were obtained with a scanning electron microscope FEI Quanta 650 F and the high-resolution images with a FEI Magellan 400 L. FTIR spectroscopy and surface charge properties were performed on a Bruker Tensor 27/PMA 50 Spectrometer and a Malven Zetasizer Nano analyzer, respectively.

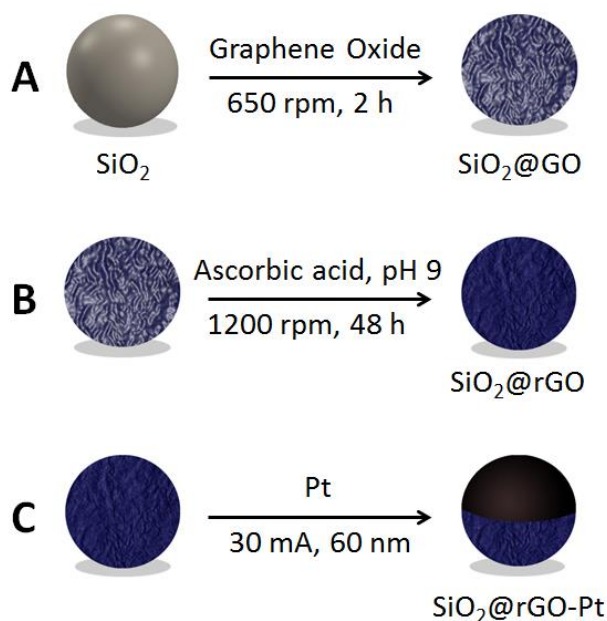


**Figure S1.** Schematic detailing the fabrication steps in the preparation of SiO<sub>2</sub>@rGO-Pt micromotors.

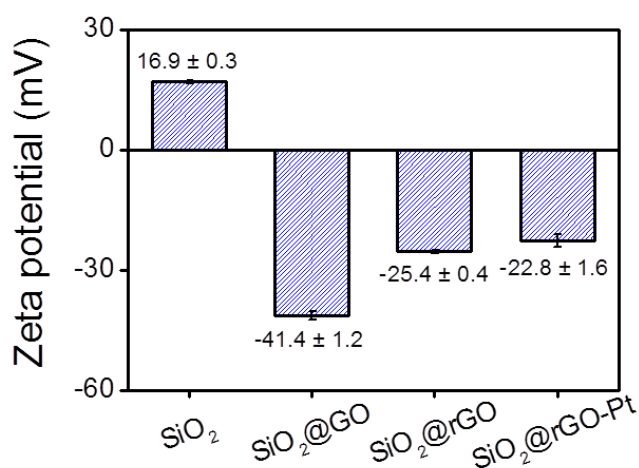


**Figure S2.** Zeta-potential values of SiO<sub>2</sub>, SiO<sub>2</sub>@GO, SiO<sub>2</sub>@rGO and SiO<sub>2</sub>@rGO-Pt, microparticles.

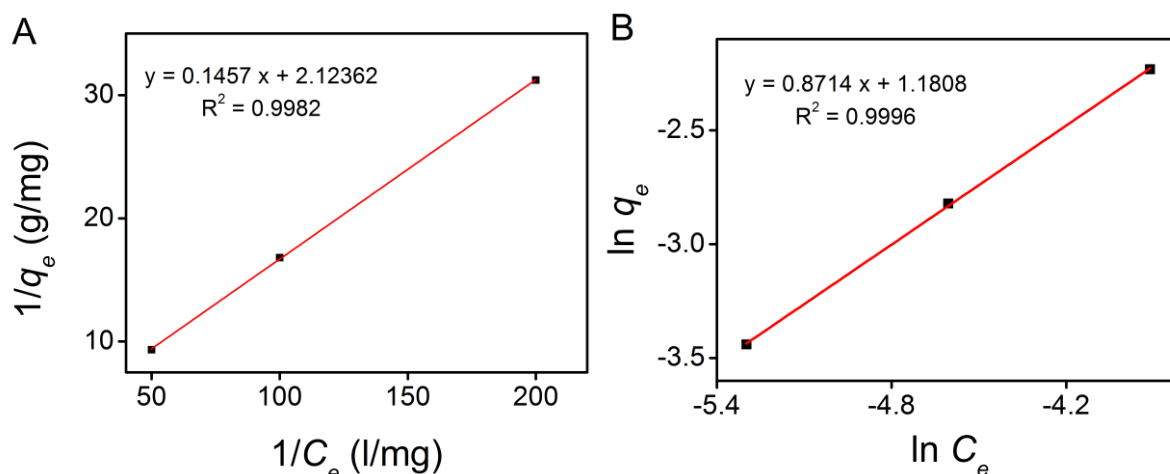


**Figure S3.** (A) Langmuir and (B) Freundlich isotherm plots for PBDEs at SiO<sub>2</sub>@rGO-Pt micromotors. Conditions: 10<sup>6</sup> micromotors in a total volume of 500  $\mu$ l, 10 ppb PBDEs, 1.5 % H<sub>2</sub>O<sub>2</sub> and 3% NaCh, 10 min reaction time.

**Table S1.** Rate constants and correlation coefficients of the pseudo-second-order kinetic model.

[PBDEs] (ppb)	$q_e$ (mg g <sup>-1</sup> )	$K_2$ (g mg <sup>-1</sup> min <sup>-1</sup> )	$V_0$ (mg g <sup>-1</sup> min <sup>-1</sup> )*	R <sup>2</sup>
5	40.7	0.009	14.4	0.9960
10	78.1	0.004	25.3	0.9974
20	140.8	0.002	44.6	0.9973

\*The initial adsorption rate  $V_0$  can be determined from the equation  $V_0 = k_2 q_e^2$ .<sup>[5]</sup>

## References

- [1] P. Šálek, L. Korecká, D. Horák, E. Petrovský, J. Kovářová, R. Metelka, M. Čadková, Z. Bílková, *J. Mater. Chem.* **2011**, *21*, 14783.
- [2] W. Shelver, L. Kamp, J. Church, F. Rubio, *J. Agric. Food Chem.* **2007**, *55*, 3758.
- [3] W. Liu, S. a Andrews, M. I. Stefan, J. R. Bolton, *Water Res.* **2003**, *37*, 3697.
- [4] L. Kantiani, M. Farré, D. Asperger, F. Rubio, S. González, M. J. López de Alda, M. Petrović, W. L. Shelver, D. Barceló, *J. Hydrol.* **2008**, *361*, 1.
- [5] H. Sun, L. Cao, L. Lu, *Nano Res.* **2011**, *4*, 550.